Supporting Information

Minor Alkyl Modifications for Manipulating Fluorescence and Photomechanical Properties in Molecular Crystals

Pengyu Li,[+] *Junxiao Wang,*[+] *Pengfei Li, Liming Lai, and Meizhen Yin**

Beijing Advanced Innovation Center for Soft Matter Science and Engineering, State Key Laboratory of Chemical Resource Engineering, Beijing Laboratory of Biomedical Materials, Beijing University of Chemical Technology, Beijing, 100029, P.R. China

E-mail: yinmz@mail.buct.edu.cn

Materials and Instruments

All chemical materials were purchased from commercial sources and used without further purification unless otherwise noted. 1H NMR and 13C NMR spectra were recorded on a Bruker 400 (400 MHz) spectrometer at room temperature with CDCl3 as the solvent and tetramethylsilane (TMS) as the internal standard. UV-Vis spectra were obtained on a spectrometer (UV-2600). Fluorescence spectroscopic studies were performed on a fluorescence spectrophotometer (Horiba JobinYvon FluoroMax-4 NIR, NJ, USA). The contribution of each lifetime and fluorescence quantum yield was recorded using an Edinburgh Instruments' FLS 980 fluorescence spectrometer. Powder X-ray diffraction (PXRD) patterns of the powder were measured using a Rigaku 2500VB2 + PC diffractometer using Cu Ka radiation (λ = 1.541844 Å) at 40 kV and 50 mA in the step-scanned mode at 0.041 (2θ) per step and at a count time of 10 s per step in the range from 5° to 40°. Differential Scanning Calorimetry (DSC) was studied using DSC Q200 (TA Instruments), under N2 flow with a heating rate of 10 oC min-1 in aluminum T-Zero pans. The morphology was investigated by field emission scanning electron microscopy (HITACHI S-4700, Japan). Single crystal X-ray diffraction data were collected with a NONIUS KappaCCD diffractometer with graphite monochromator and Mo

Kα radiation [λ (MoKα) = 0.71073 Å]. Structures were solved by direct methods with SHELXS-97 and refined against F2 with SHELXS-97.

Computational details

The aggregation effect was considered by using ONIOM method with QM and MM layers in Gaussian 09 program. The UFF force field was used with the restrained electrostatic potential (RESP) partial charges for the MM treatment. And the computation model for solid phase was built by digging a cluster from the X-ray crystal structures and two monomer and three pai-dimers were further defined the as QM, respectively. All calculations of energy level for the ground state (S0) and the first excited state (S1) were respectively studied by using the restricted density functional theory (DFT) and TD-DFT by B3LYP hybrid functional combined with 6-31G+(d,p) basis sets.

Non-covalent interaction (NCI) analysis was performed through Multiwfn_3.8 program.

The free volumes of two crystals were calculated in Material Studio software package and the FFV value were calculated by the following equation:

$$FFV\ \% = \frac{V_F}{V_F + V_O}$$

Where V_F is the value of free volume and Vo is the value of occupied volume.

The Hirshfeld surfaces and energy frameworks in two crystlas were calculated in CrystalExplorer software package.

Synthesis and Characterizations of CSEt or CSPr

The detailed synthesis routes is shown in Scheme S1 and the synthesis of CS-COOH was carried out according to the previous literature. Adding CS-COOH (295 mg, 1.0 mmol) and 10 mL ethonal (EtOH) in 50 mL reaction flask, and 0.2 mL concentrated sulfuric acid (H2SO4) was added deopwise with stirring. After refluxing at 90 ℃ for 24 h, cooling the reaction system to room temperature. Pouring the reaction mixture into 100mL deionized water and performing vacuum suction filtration. The residue was purified by chromatography (dichloromethane as eluant) to give CSEt or CSPr of yellowish powders (342 mg, yield 98 % for CSEt and 358 mg, yield 95% for CSPr).

Characterization of CSEt: ^{1}H NMR (400 MHz, Chloroform-d) δ 8.14 (t, J = 8.5 Hz, 4H), 7.97 (d, J = 8.3 Hz, 2H), 7.77 (d, J = 8.4 Hz, 2H), 7.66 (s, 1H), 4.42 (q, J = 7.1 Hz, 4H), 1.42 (t, J = 7.1 Hz, 6H).

^{13}C NMR (101 MHz, CDCl3) δ 165.76, 165.70, 142.39, 138.02, 137.23, 132.29, 131.44, 130.35, 130.15, 129.32, 126.05, 117.15, 113.04, 77.36, 77.04, 76.73, 61.37, 61.35, 14.33, 14.31, 0.00.

Characterization of CSPr: ^{1}H NMR (400 MHz, Chloroform-d) δ 8.14 (t, J = 8.3 Hz, 4H), 7.97 (d, J = 7.9 Hz, 2H), 7.77 (d, J = 8.0 Hz, 2H), 7.66 (s, 1H), 4.32 (t, J = 6.7 Hz, 4H), 1.82 (h, J = 7.2 Hz, 4H), 1.05 (t, J = 7.4 Hz, 6H). ^{13}C NMR (101 MHz, CDCl3) δ 165.81, 165.76, 142.39, 138.03, 137.24, 132.32, 131.47, 130.35, 130.15, 129.33, 126.07, 117.15, 113.06, 77.35, 77.03, 76.72, 66.94, 66.91, 22.10, 10.52.

Photosynthesis of *d*-CSEt

After the ultrasound treatment in *n*-hexane, the CSEt microcrystal powder (100 mg) is laid on glass plate and irradiated with hand-hold UV lamp (50 mW/cm2) for 4 h. Then, the UV irradiated powder was purified by chromatography method (dichloroethane/methnol = 50/1 mixture as eluant) to give *d*-CSEt of a white powder (50 mg, yield 50%). 1H NMR (400 MHz, Chloroform-d) δ 8.00 – 7.95 (m, 8H), 7.37 (d, J = 8.5 Hz, 4H), 7.31 (d, J = 8.4 Hz, 4H), 5.30 (s, 2H), 4.37 (q, J = 7.1 Hz, 8H), 1.38 (t, J = 7.1 Hz, 12H).

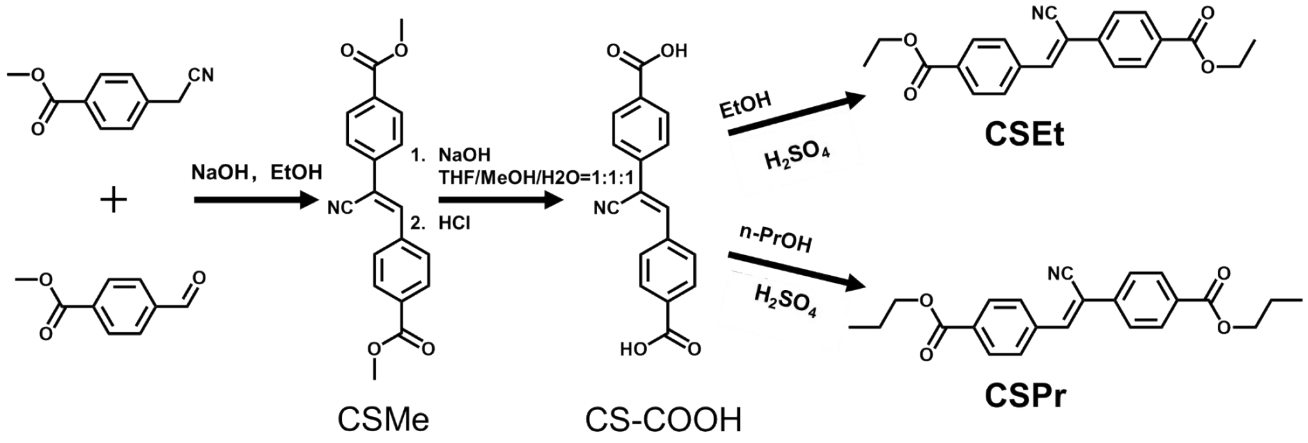

Scheme S1. Synthesis routes of CSEt and CSPr.

Table S1. Crystal data and structure refinement for CSEt.

Identification code	**CSEt**	**CSPr**	**d-CSEt**
CCDC number	1983911	1983900	2034901
Empirical formula	$C_{21}H_{19}NO_4$	$C_{23}H_{23}NO_4$	$C_{42}H_{38}N_2O_8$
Formula weight	349.37	377.42	698.74
Temperature / K	107.85(10)	110.1(9)	296.15
Crystal system	triclinic	triclinic	triclinic
Space group	*P*-1	*P*-1	*P*-1
a / Å **b / Å** **c / Å**	8.8112(11) 9.4028(11) 11.1812(11)	6.6609(7) 7.3282(7) 21.588(2)	8.219(2) 12.255(3) 18.230(5)
α/° **β/°** **γ/°**	97.718(9) 108.562(10) 93.381(10)	85.693(9) 83.663(9) 69.364(9)	82.115(7) 83.731(7) 85.635(7)
Volume / Å^3	865.11(17)	979.40(17)	1804.4(8)
Z	2	2	2
ρ_{calc} / mg mm^{-3}	1.341	1.280	1.286
μ / mm^{-1}	0.093	0.087	0.089
F(000)	368	400	736.0
2θ range for data collection	6.32 to 52°	6.18 to 52°	4.292 to 55.204
Index ranges	$-10 \le h \le 9$ $-11 \le k \le 11$ $-13 \le l \le 13$	$-7 \le h \le 8$ $-7 \le k \le 9$ $-26 \le l \le 26$	$-10 \le h \le 10$ $-15 \le k \le 15$ $-19 \le l \le 23$
Reflections collected	6190	7347	14041
Independent reflections	3396[R(int) = 0.0254 (inf-0.9Å)]	3835[R(int) = 0.0237 (inf-0.9Å)]	8152 [Rint = 0.0378, Rsigma = 0.0610]
Data/restraints/parameters	3396/0/237	3835/0/255	8152/0/473
Goodness-of-fit on F^2	1.040	1.031	1.017
Final R indexes [I>2σ (I) i.e. F_o>4σ (F_o)]	R_1 = 0.0572, wR_2 = 0.1265	R_1 = 0.0440, wR_2 = 0.0973	R1 = 0.0567, *w*R2 = 0.1337
Final R indexes [all data]	R_1 = 0.0717, wR_2 = 0.1372	R_1 = 0.0551, wR_2 = 0.1041	R1 = 0.0922, *w*R2 = 0.1545
Largest diff. peak/hole / e Å^{-3}	0.850/-0.320	0.246/-0.206	0.33/-0.22
Flack Parameters	N	N	2

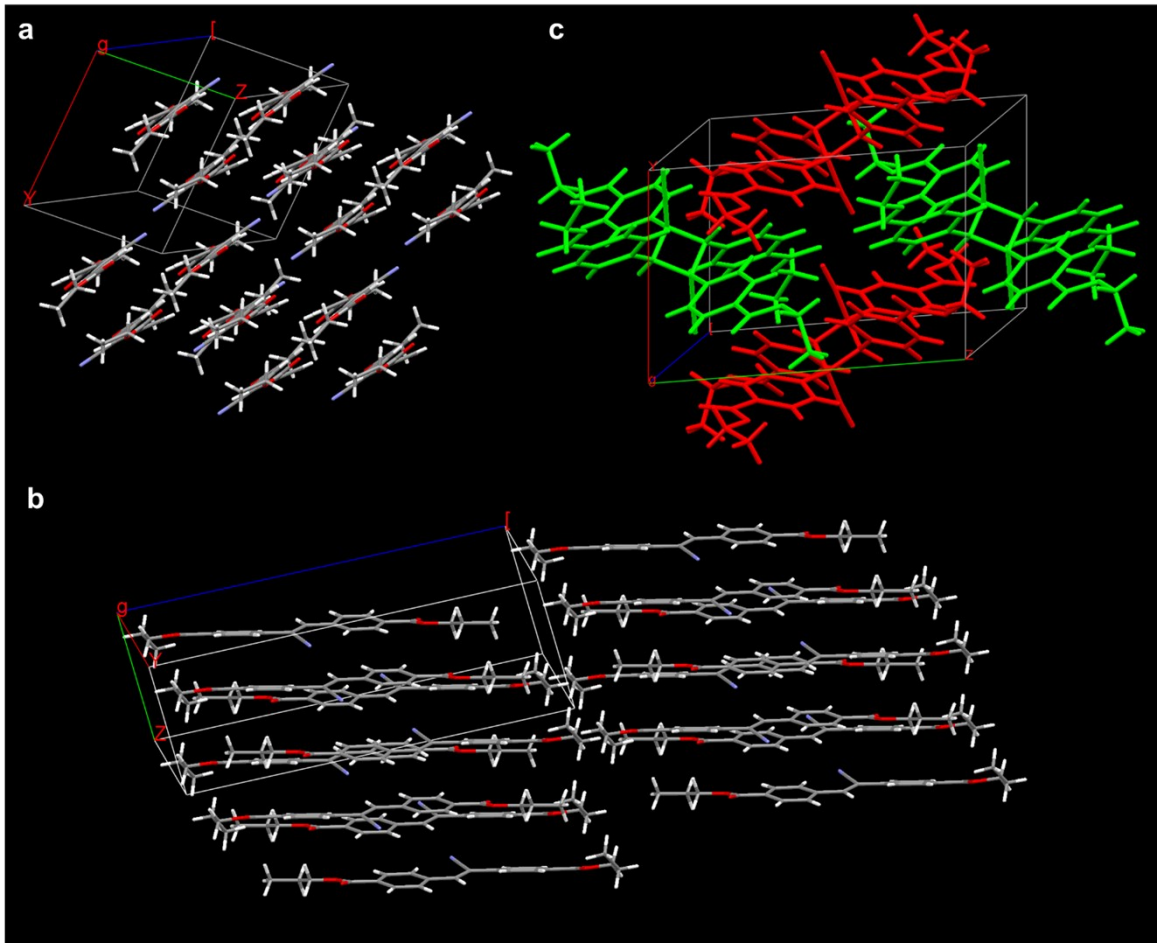

Figure S1. Crystal structure of (a) CSEt and (b) CSPr in 2*2*2 lattice. (c) Crystal structure of d-CSEt, the two chiral enantiomers were labelled by red and green, respectively.

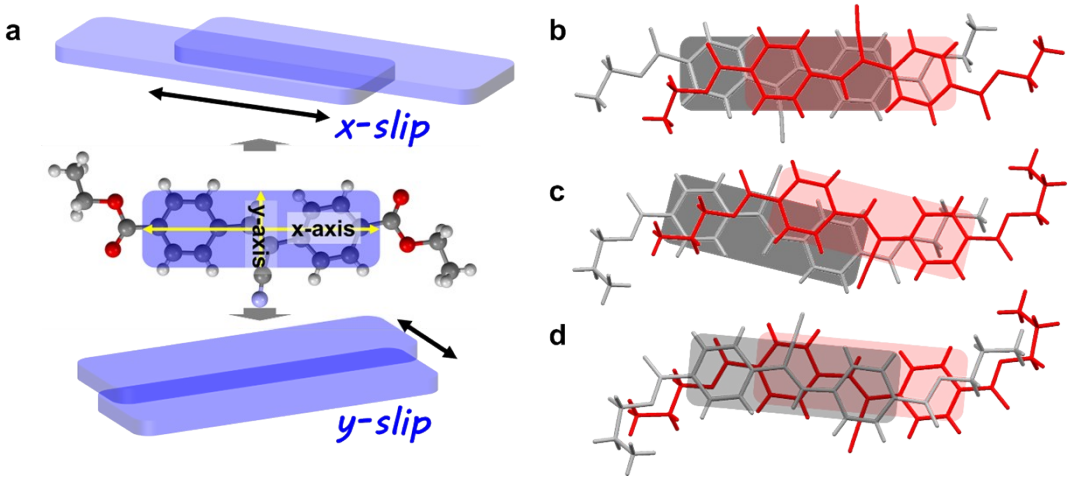

Figure S2. (a) Schematic illustrations of the intermolecular slipping modes. The dimer structures of (b) CSEt dimer, (c) CSPr dimer 1 and (d) CSPr dimer 2 with the illustrations of respective π-planar overlaps.

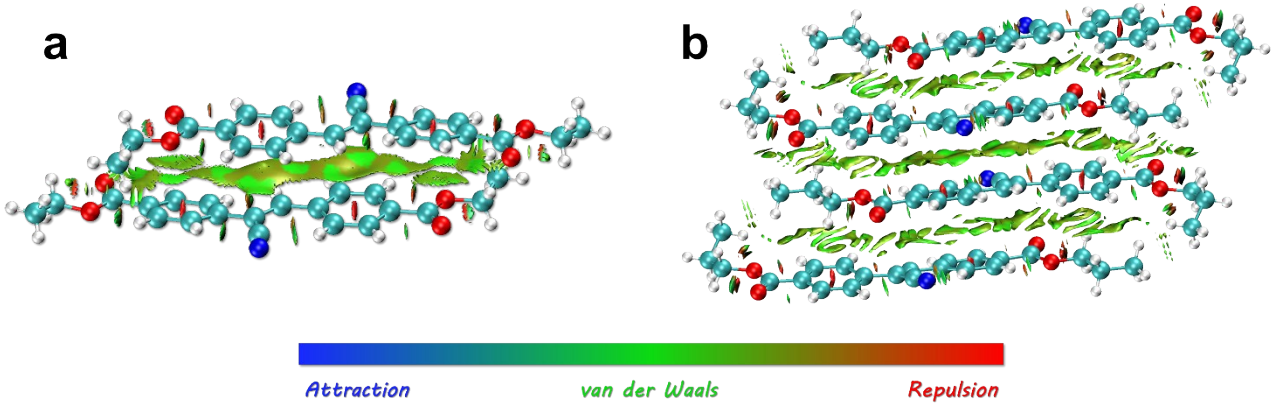

Figure S3. Non-covalent interactions analysis of (a) CSEt dimer and (b) CSPr tetramer.

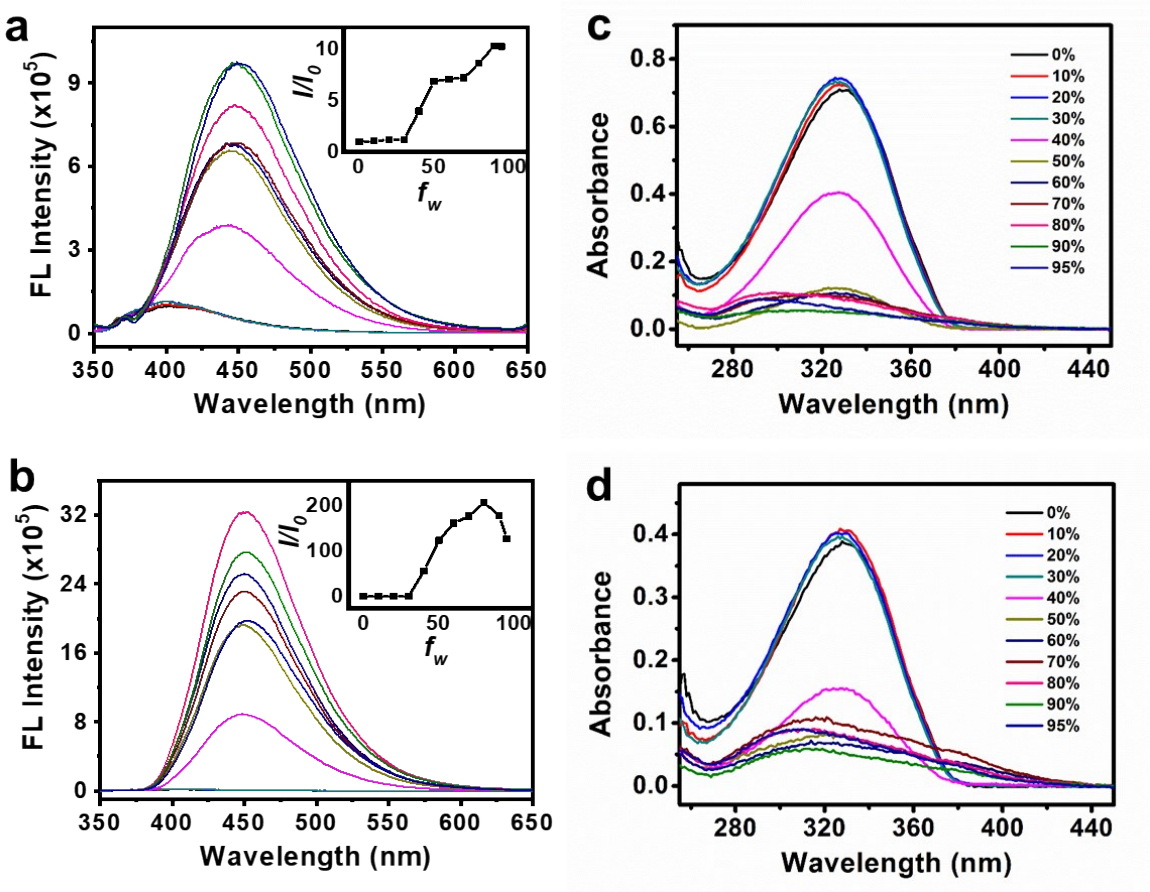

Figure S4. Fluorescence and absorption spectra of CSEt (a, c) and CSPr (b, d) in DMSO/H_2O solutions with various f_w (Insets of a and c are the curve of fluorescence enhancement).

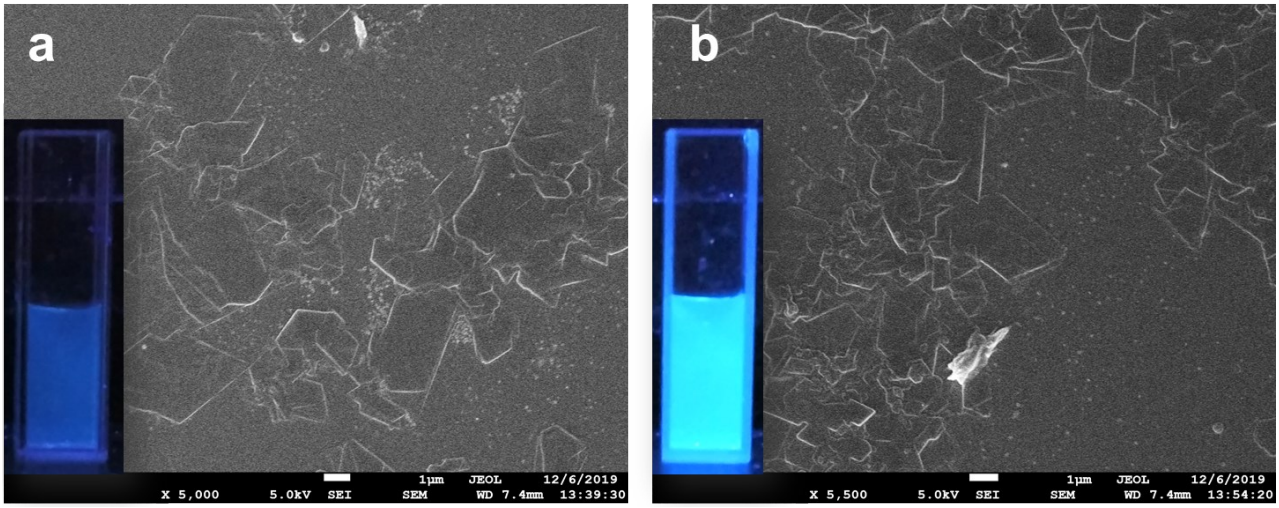

Figure S5. The SEM images of amorphous aggregates of CSEt (a) and CSPr (b).

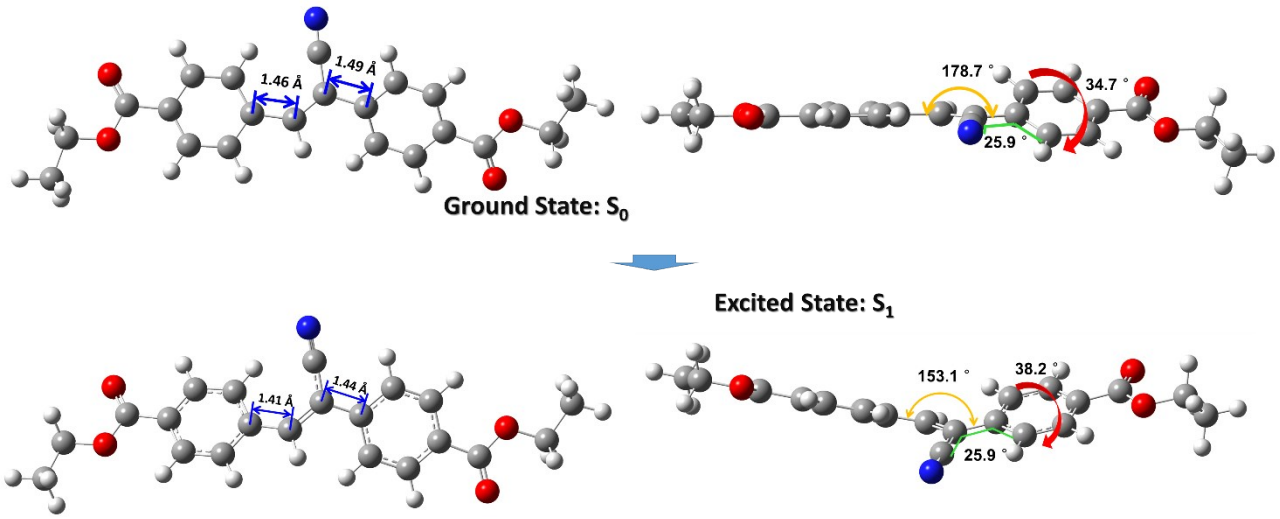

Figure S6. The conformations of CSEt molecule in ground and excited state simulated based on b3LYP/6-31*(d,p) at gas state.

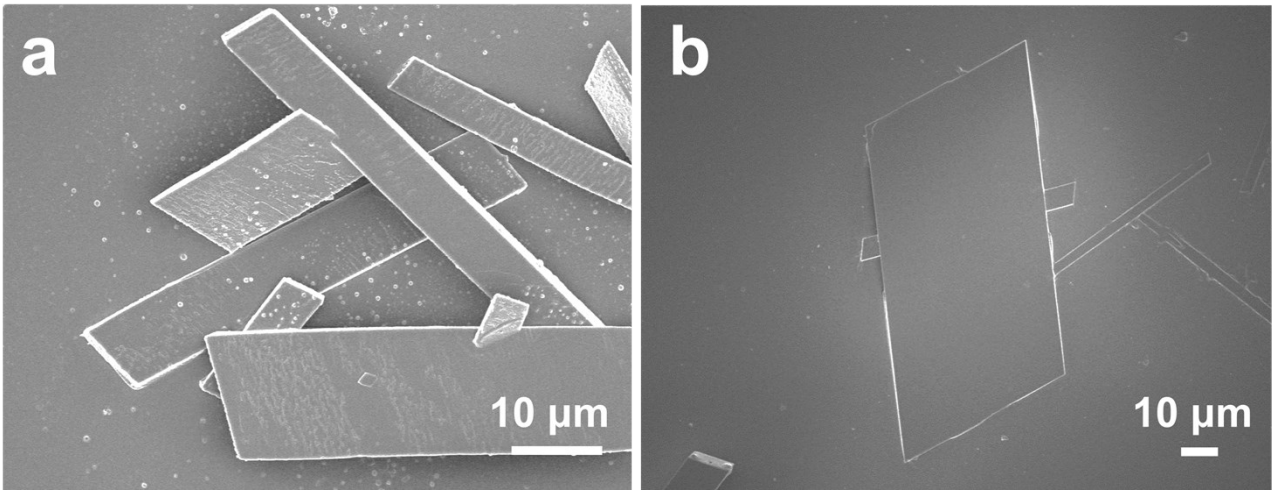

Figure S7. SEM images of (a) CSEt and (b) CSPr crystal.

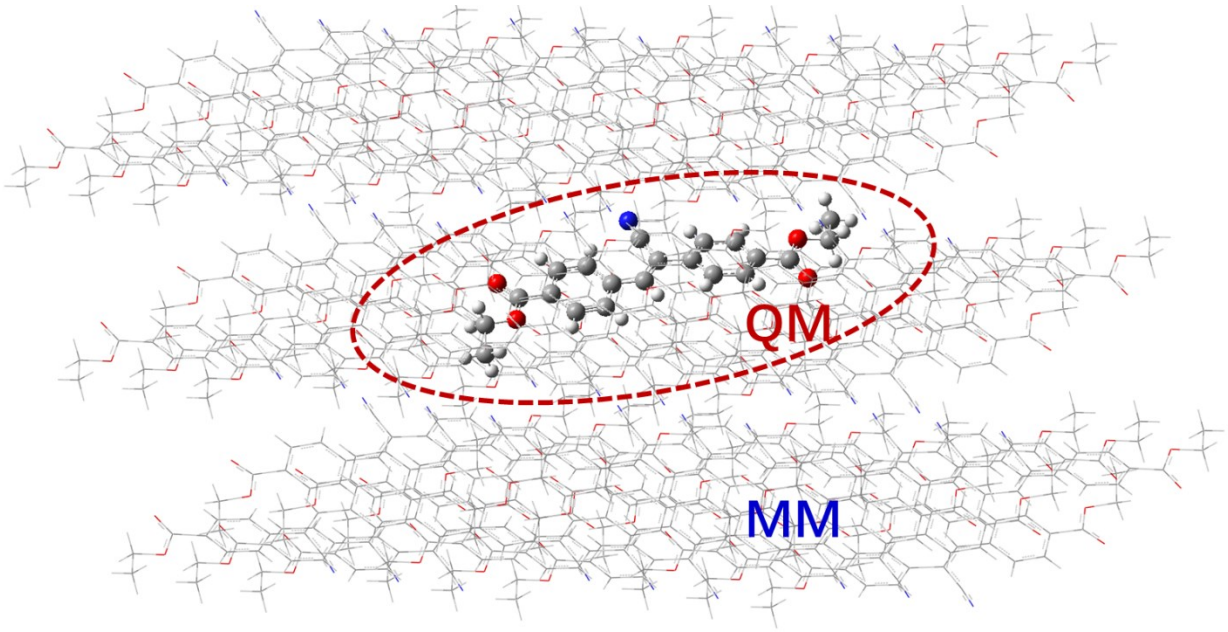

Figure S8. QM/MM model of CSEt monomer as an example. 54 molecules are included and the central one is treated as QM part and the surrounding molecules act as the MM parts. In the geometry optimization, the QM part is active and the MM part is frozen.

¥

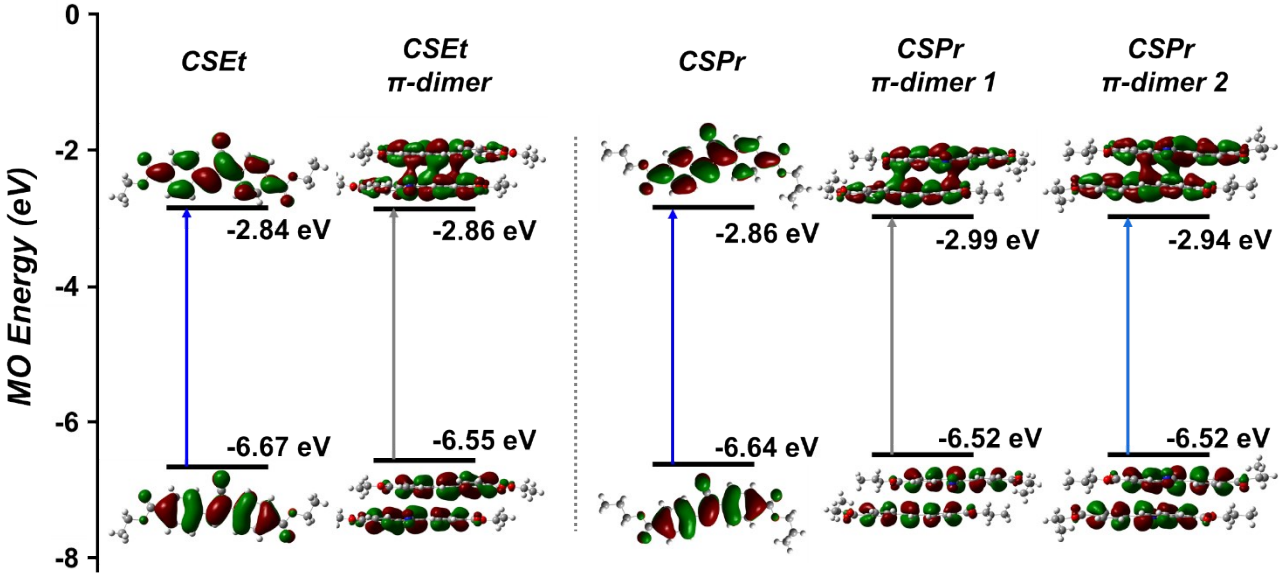

Figure S9. HOMO and LUMO distributions of the monomers and dimers from CSEt and CSPr crystals, respectively.

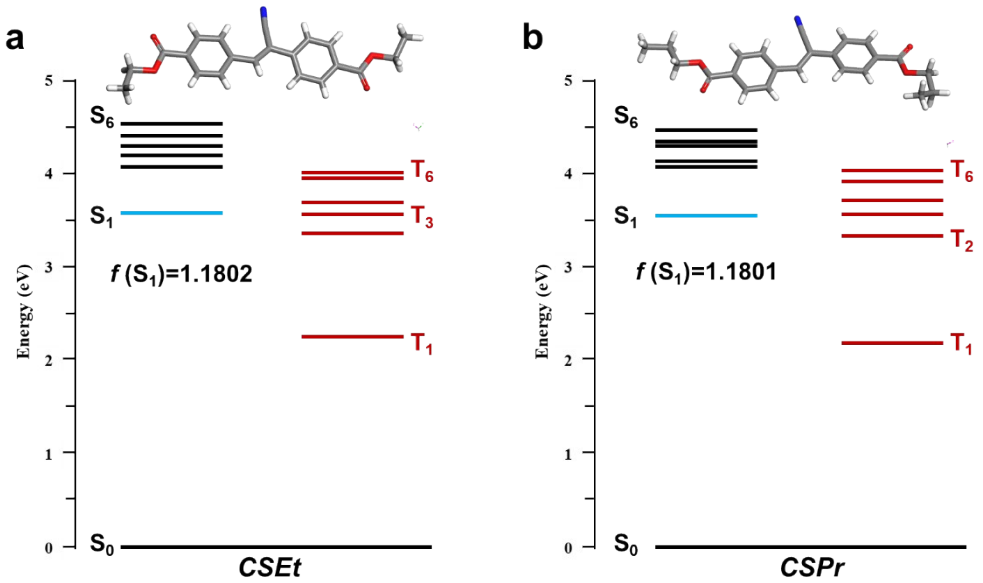

Figure S10. TD-DFT calculated energy diagrams of CSEt and CSPr monomers.

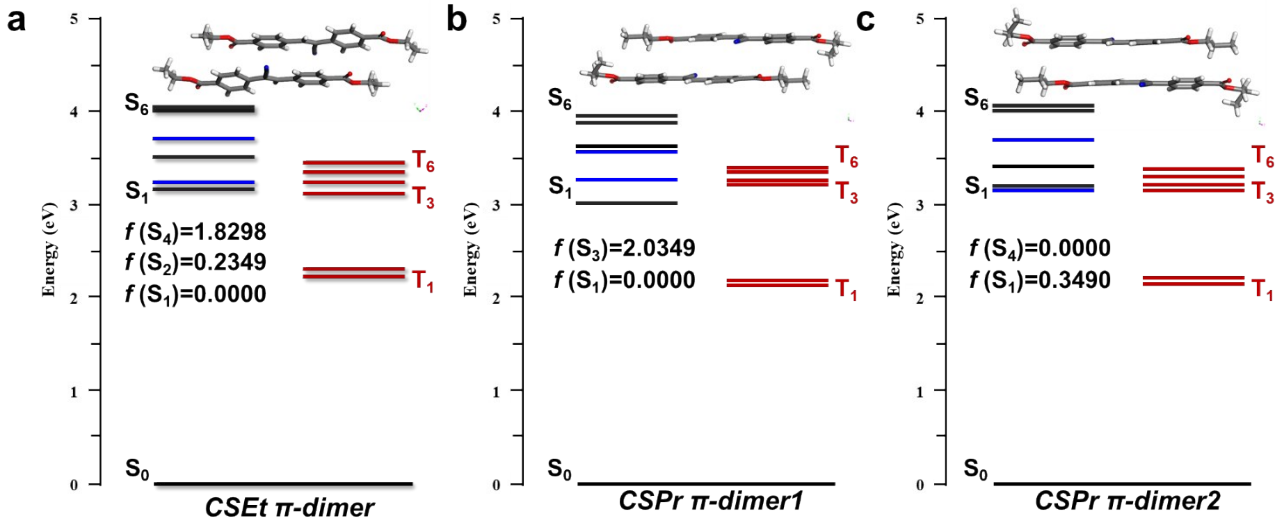

Figure S11. TD-DFT calculated energy level of CSEt and CSPr dimers.

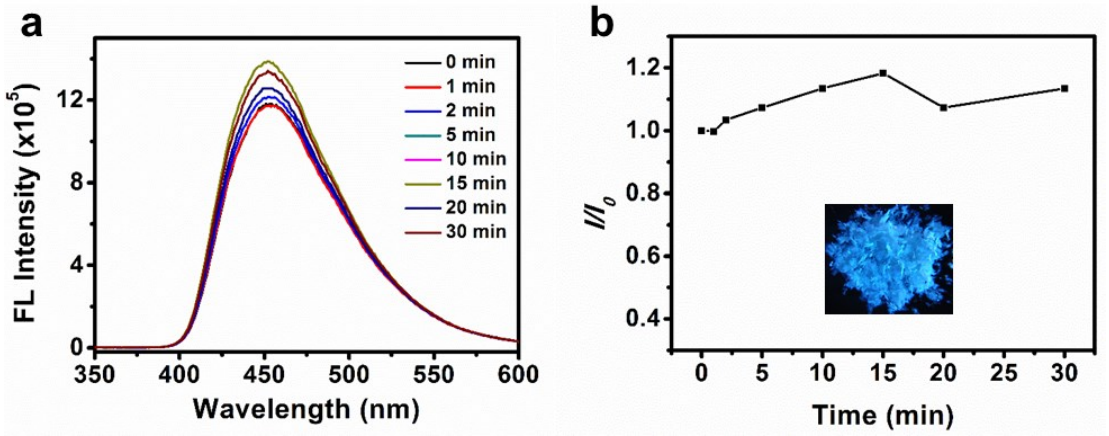

Figure S12. Time-dependent (a) fluorescence spectra and (b) plots of relative maximum fluorescence intensity (I/I_0) of CSPr crystal under continuous UV irradiation.

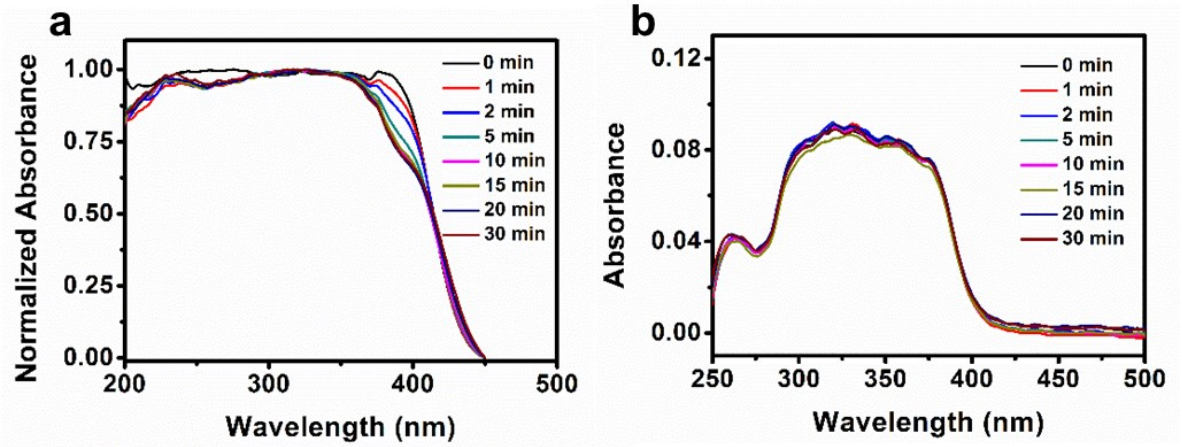

Figure S13. Time-dependent solid-state absorption spectra of CSEt (a) and CSPr (b) crystal under continuous UV irradiation.

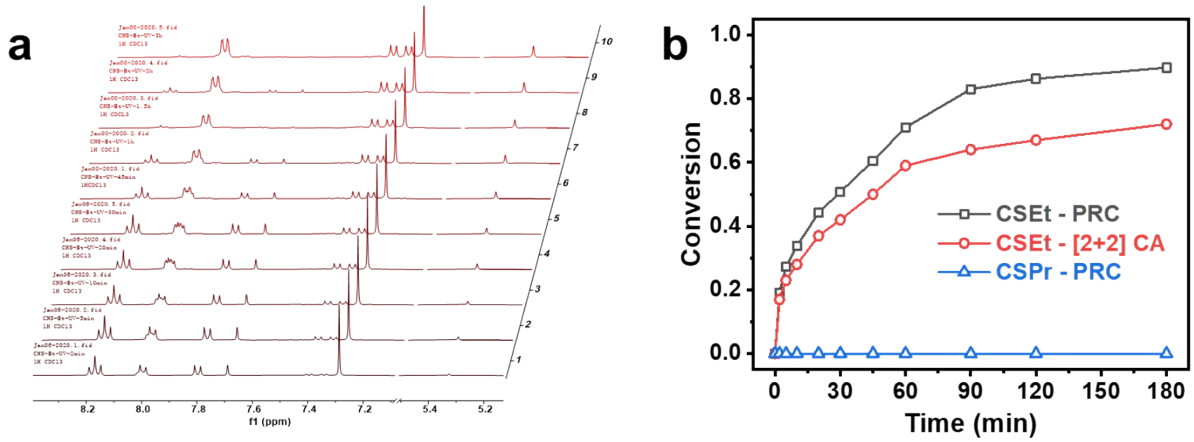

Figure S14. (a) Partial ^{1}H NMR spectra monitoring the photoreaction process of CSEt crystal under UV irradiation. (b) Photoreaction conversion (PRC) of CSEt and CSPr and productivity of [2+2] cycloaddition (CA) product.

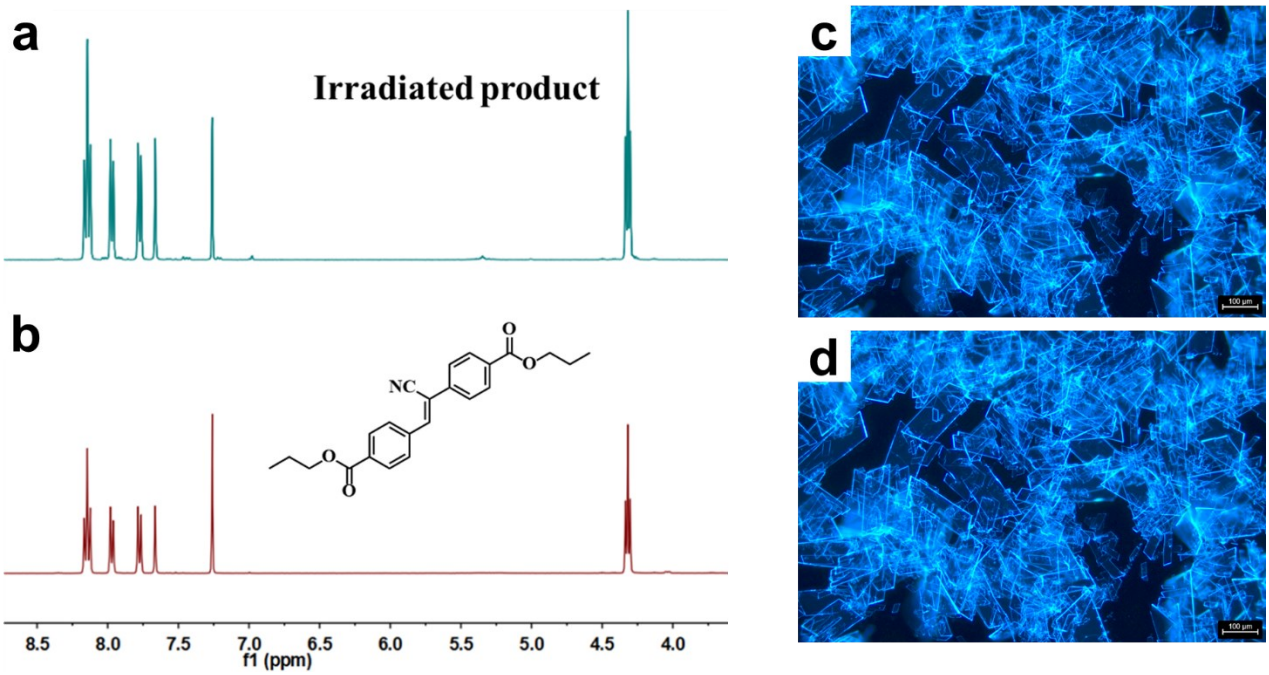

Figure S15. Partial ^{1}H NMR spectra of CSPr crystal (a) before and (c) after UV irradiation for 30 min. Fluorescent photographs of CSPr crystal (c) and (d) after UV irradiation for 10 min.

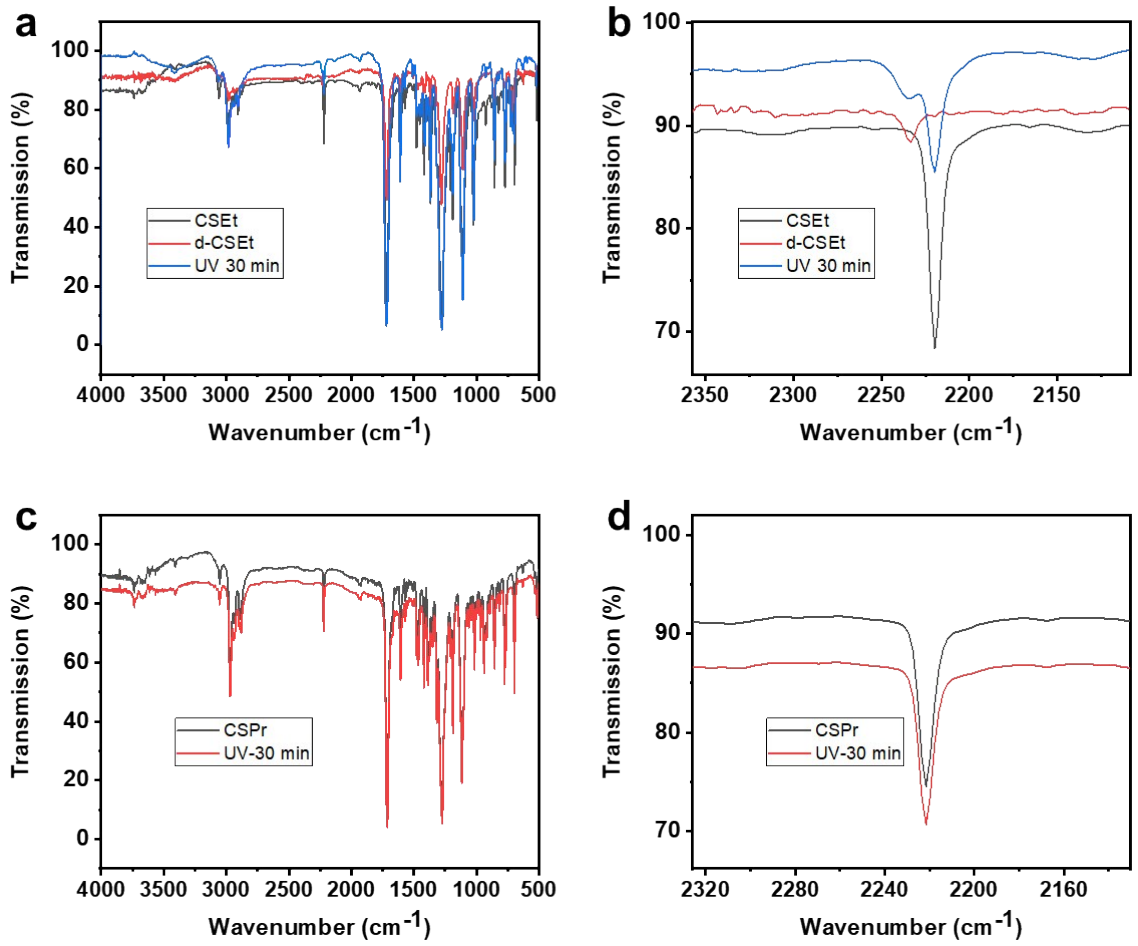

Figure S16. FT-IR spectra of (a, b) CSEt and (c, d) CSPr crystals: (a, c) full spectra. (b, d) Partial of (a) and (c).

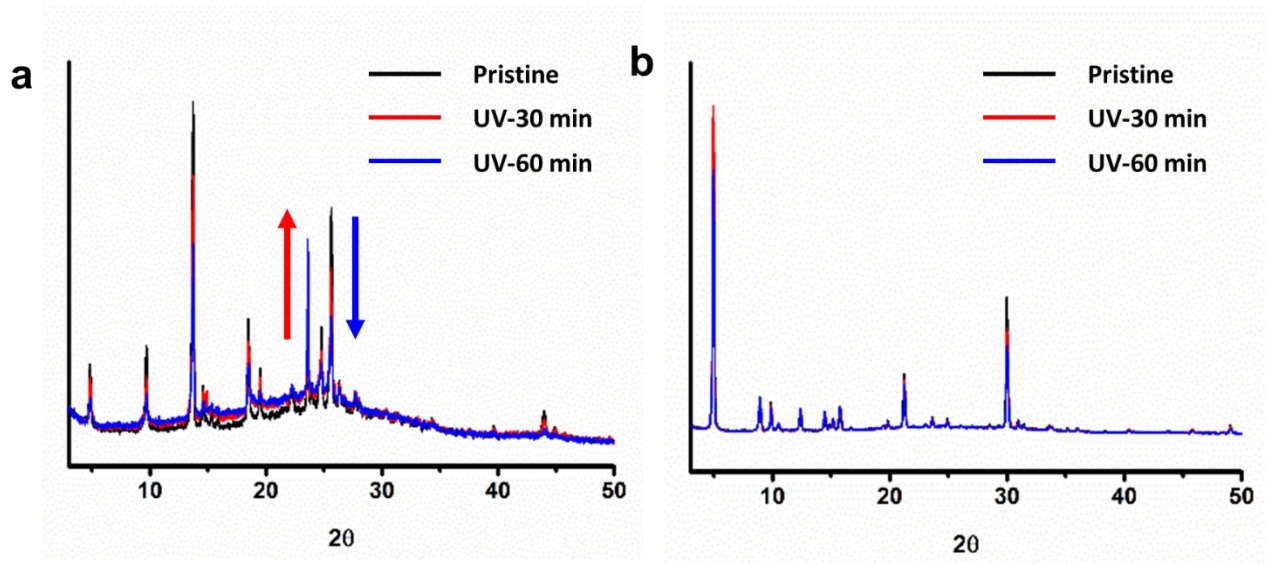

Figure S17. Time-dependent PXRD patterns of CSEt (a) and CSPr (b) crystals irradiated with hand-hold UV lamp for different time.

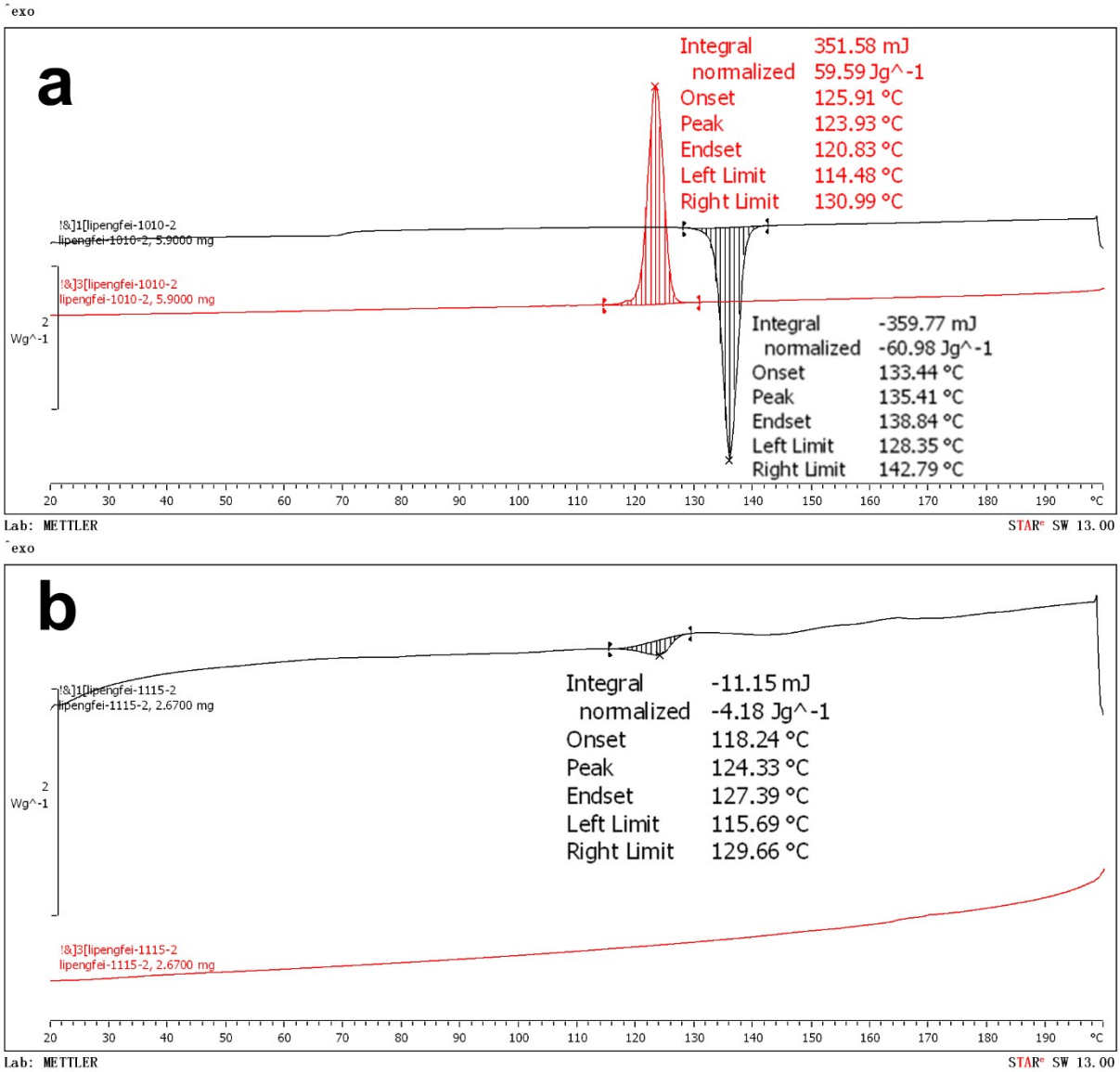

Figure S18. DSC curves of CSEt crystal before (a) and after (b) UV irradiation for 15 h with hand-hold UV lamp.

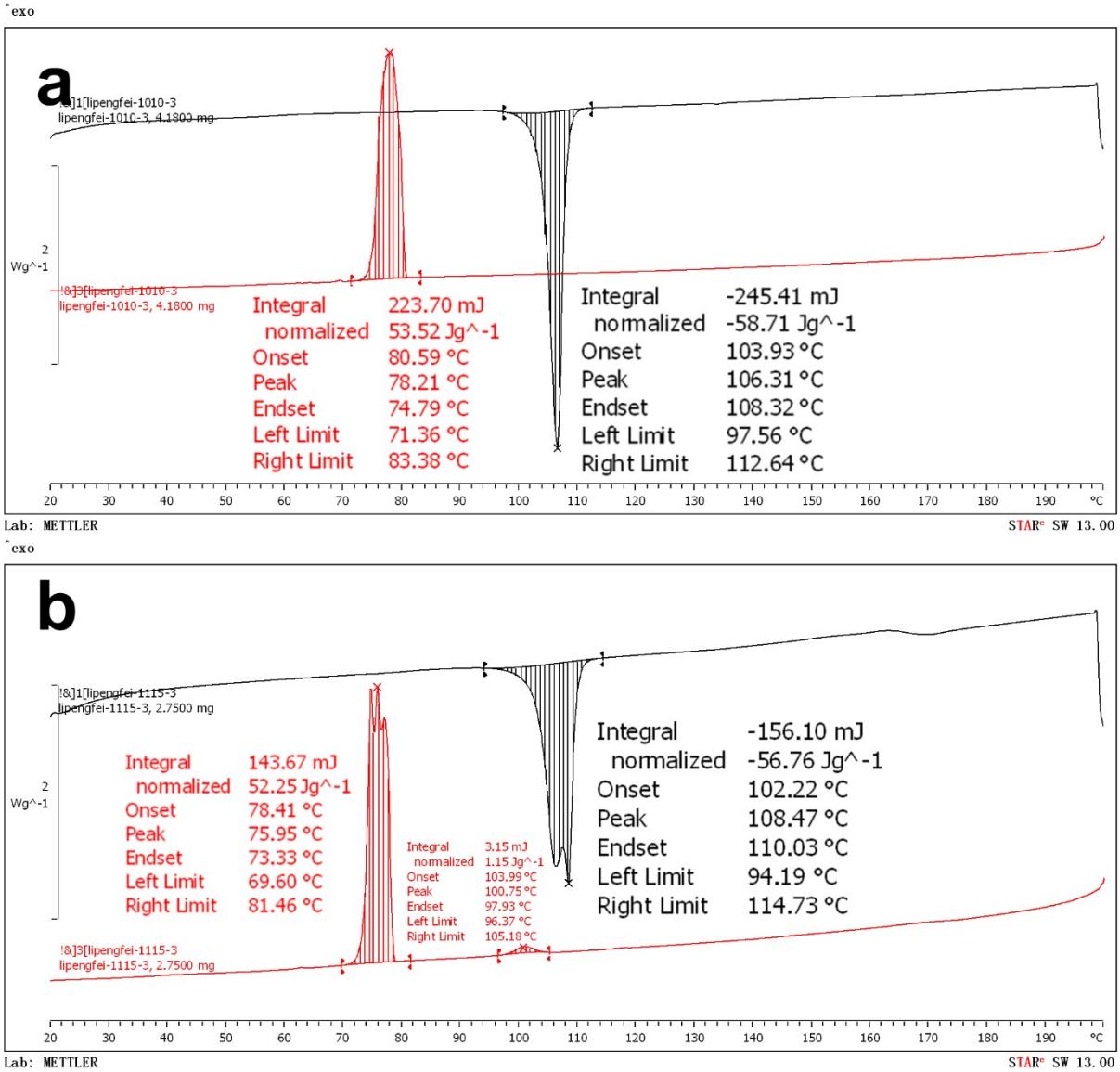

Figure S19. DSC curves of CSPr crystal before (a) and after (b) UV irradiation for 15 h with hand-hold UV lamp.

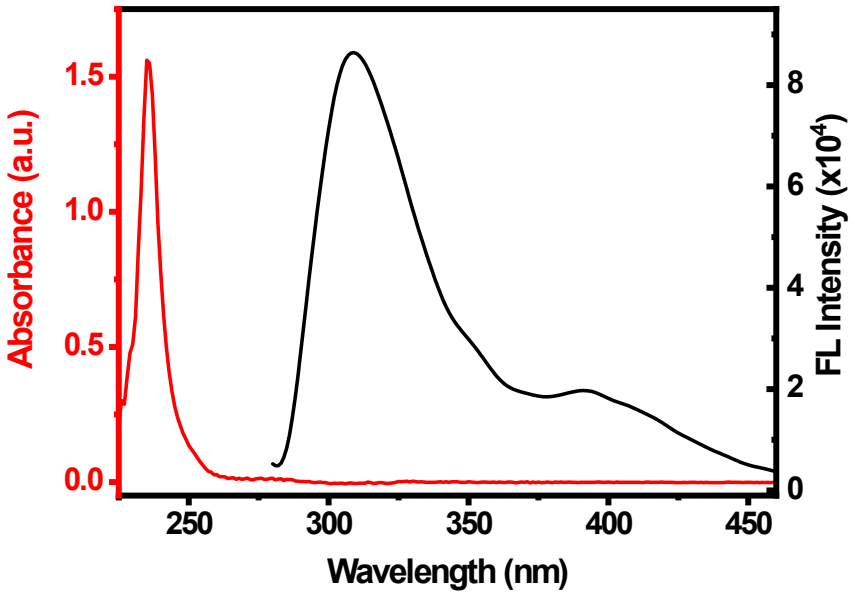

Figure S20. Absorption and fluorescence spectra of *d*-CSEt (Concentration: 2×10^{-5} M).

Table S2. Geometric parameters of CSEt and CSPr dimers for [2 + 2] cycloaddition.

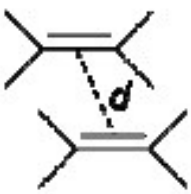

Dimer	*d*/Å	θ_1/°	θ_2/°	θ_3/°
ideal	<4.2	0	90	90
CSEt	4.687	0	52.11	61.29
CSPr 1	6.208	0	64.98	40.61
CSPr 2	4.670	0	56.89	58.21

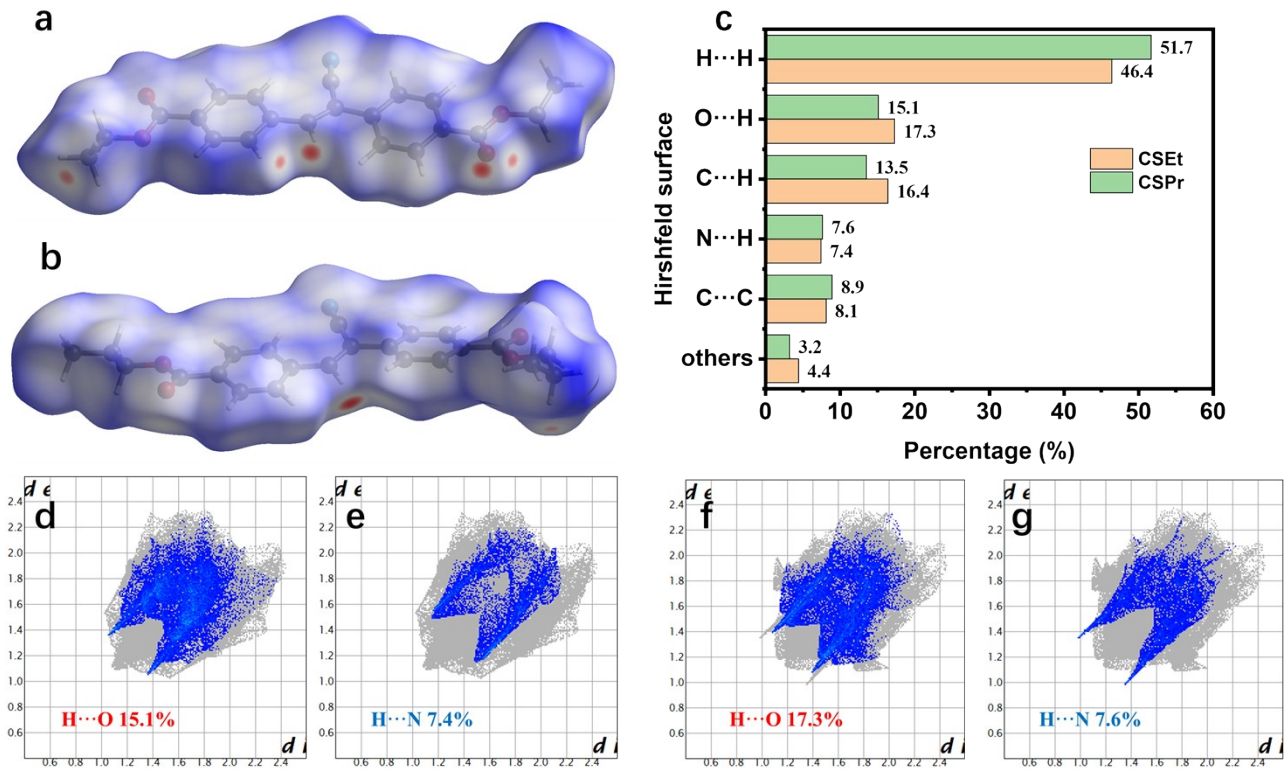

Figure S21. Hirshfeld surface of crystals CSEt (a) and (b) CSPr. (c) Individual atomic contact percentage contribution to the Hirshfeld surface in CSEt and CSPr crystals. 2D fingerprint plot of H···O and H···N interactions of crystals (d,e) CSEt and (f,g) CSPr.

The red areas on the surfaces represent the O···H interactions of CSEt and the N···H interactions of CSPr, respectively, exhibiting relevant sharp spikes in the 2D fingerprint plots. The H···H interactions takes the highest proportions, exhibiting that the van der Waals interactions are the major factor for the crystallizations (Fig. S21c). Meanwhile, the H···H interactions cover 51.7% of Hirshfeld surfaces of CSPr, higher than 46.4% of CSEt, which is attributed to the more contact among the propyl groups between the molecular layers in CSPr crystal. The plots of O···H interactions in CSEt crystal are more disperated than that in CSPr crystal, indicating the distinct O···H interactions environments. The plots of N···H interactions in CSPr crystal locates at small di and de region, indicating the stronger strength than that in CSEt crystal.

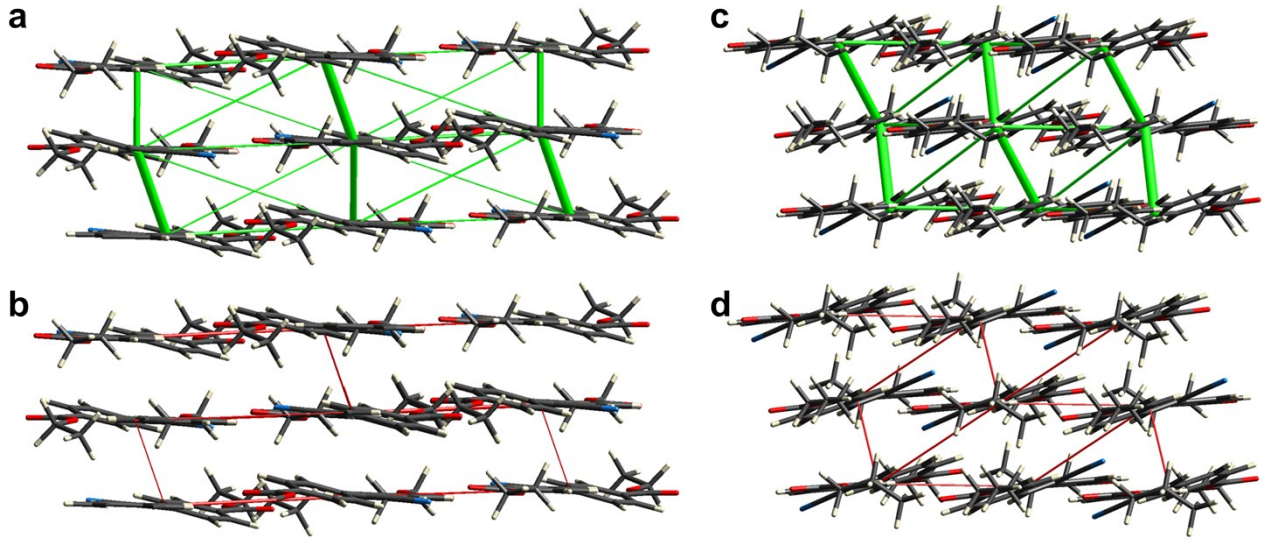

Figure S22. Energy frameworks of (a,b) CSEt and (c,d) CSPr crystals. (a,c) The disperation energy and (b,d) the coulomb energy of respective crystal.

Figure S22a and c exhibit the strong disperation energy in the dimers, which are similar to the total energy shown in Figure 6c and d, exhibiting the predominance in the crystallizations. Meanwhile, the strength out of the dimers decrease obviously. Figure S22b and d demonstrate the poor coulomb energy among the CS molecules due to the poor intramolecular charge tranfer effect.

Table S3. Interaction energy framework in CSEt crystal.

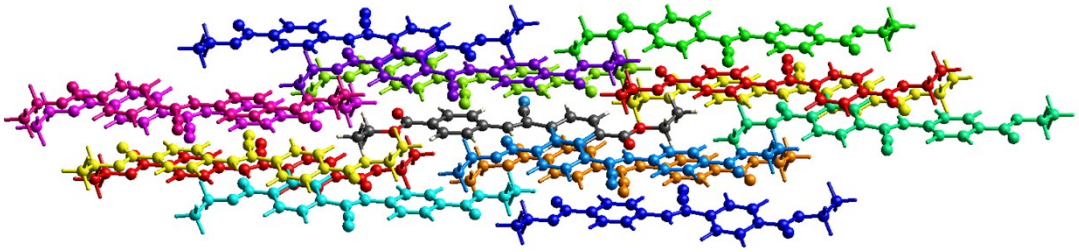

	N	Symop	R	Electron Density	E_ele	E_pol	E_dis	E_rep	E_tot
	1	x, y, z	15.55	B3LYP/6-31G(d,p)	-5.6	-1.5	-17.4	8.4	-17.0
	0	-x, -y, -z	7.42	B3LYP/6-31G(d,p)	-4.6	-1.7	-75.3	37.1	-48.8
	0	x, y, z	16.32	B3LYP/6-31G(d,p)	-1.6	-0.3	-16.2	10.7	-9.4
	0	-x, -y, -z	8.27	B3LYP/6-31G(d,p)	-12.0	-4.7	-16.0	14.9	-20.9
	1	-x, -y, -z	13.71	B3LYP/6-31G(d,p)	-2.9	-0.9	-9.7	2.4	-10.8
	1	-x, -y, -z	21.28	B3LYP/6-31G(d,p)	0.1	-0.6	-9.8	8.9	-3.5
	0	-x, -y, -z	10.18	B3LYP/6-31G(d,p)	-4.9	0.0	-49.4	35.8	-26.0
	1	-x, -y, -z	8.42	B3LYP/6-31G(d,p)	-31.1	-8.5	-36.7	40.0	-46.5
	0	x, y, z	11.18	B3LYP/6-31G(d,p)	-7.1	0.0	-16.5	8.7	-16.6
	1	-x, -y, -z	4.66	B3LYP/6-31G(d,p)	-10.8	-2.5	-111.3	67.8	-68.3
	0	-x, -y, -z	18.24	B3LYP/6-31G(d,p)	-14.8	-4.3	-16.9	14.1	-24.8
	0	-x, -y, -z	19.70	B3LYP/6-31G(d,p)	-0.7	-0.1	-5.5	5.8	-2.1

Interaction Energies (kJ/mol)

R is the distance between molecular centroids (mean atomic position) in Å.

Total energies, only reported for two benchmarked energy models, are the sum of the four energy components, scaled appropriately.

Table S4. Interaction energy framework in CSPr crystal.

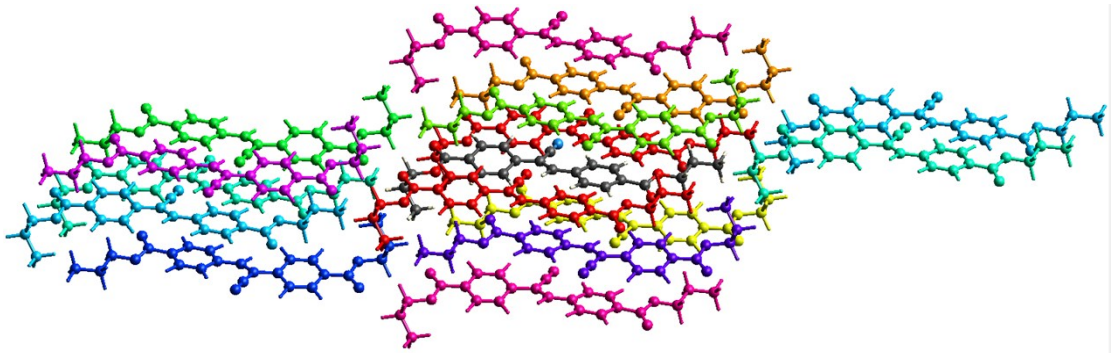

	N	Symop	R	Electron Density	E_ele	E_pol	E_dis	E_rep	E_tot
	2	x, y, z	6.66	B3LYP/6-31G(d,p)	-20.6	-6.4	-36.0	32.4	-37.9
	1	-x, -y, -z	8.09	B3LYP/6-31G(d,p)	-8.6	-3.9	-38.4	24.2	-30.4
	1	-x, -y, -z	5.85	B3LYP/6-31G(d,p)	-8.5	-2.6	-108.8	58.5	-69.5
	1	-x, -y, -z	4.69	B3LYP/6-31G(d,p)	-19.7	-2.2	-131.2	79.7	-87.5
	1	-x, -y, -z	18.40	B3LYP/6-31G(d,p)	-13.1	-4.0	-13.9	9.8	-22.8
	2	x, y, z	21.59	B3LYP/6-31G(d,p)	-0.3	-0.1	-1.5	0.0	-1.7
	2	x, y, z	23.28	B3LYP/6-31G(d,p)	0.3	-0.1	-3.6	1.5	-1.9
	1	-x, -y, -z	19.23	B3LYP/6-31G(d,p)	-1.7	-0.5	-14.0	9.6	-8.4
	1	-x, -y, -z	6.72	B3LYP/6-31G(d,p)	-16.3	-6.5	-49.5	33.5	-44.4
	1	-x, -y, -z	20.39	B3LYP/6-31G(d,p)	-0.6	-0.3	-9.7	5.1	-6.2
	2	x, y, z	7.98	B3LYP/6-31G(d,p)	-0.1	-0.5	-5.7	0.2	-5.3

Interaction Energies (kJ/mol)
R is the distance between molecular centroids (mean atomic position) in Å.
Total energies, only reported for two benchmarked energy models, are the sum of the four energy components, scaled appropriately.

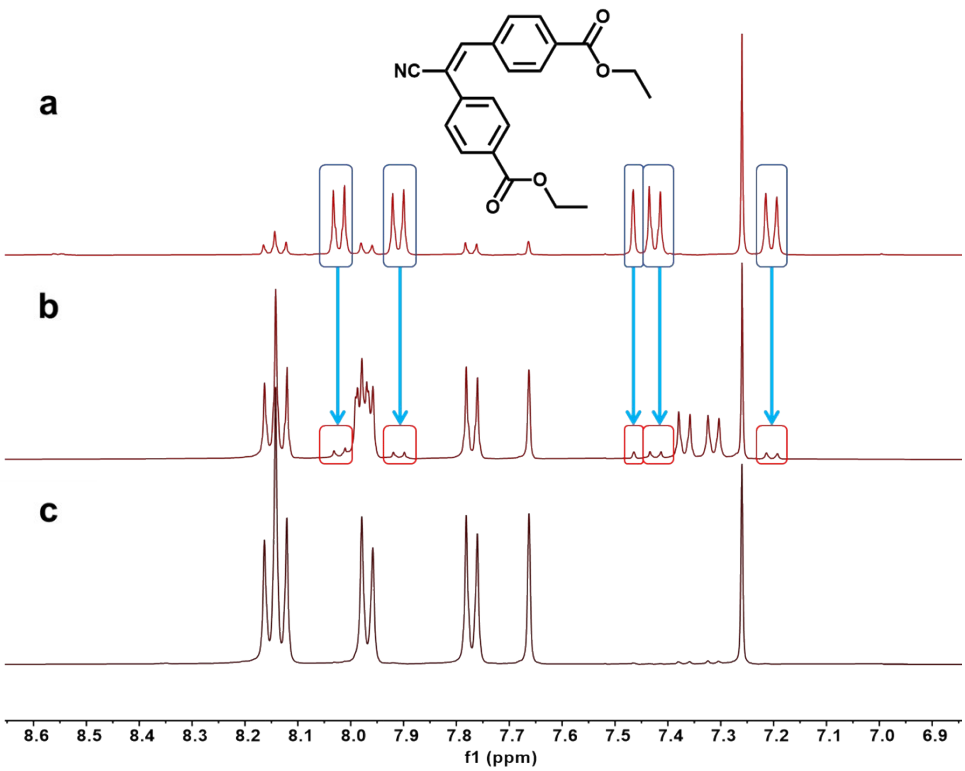

Figure S23. Partial 1H NMR spectra of CSEt in different conditions: (a) irradiated in solution. (b) irradiated in solid state. (c) without any treatment.

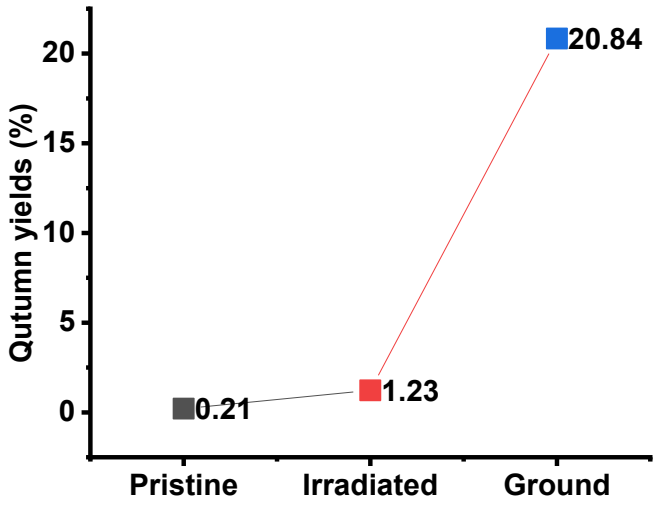

Figure S24. Fluorescence quantum yield of CSEt microcrystal in different conditions: pristine, UV irradiated and force ground samples.

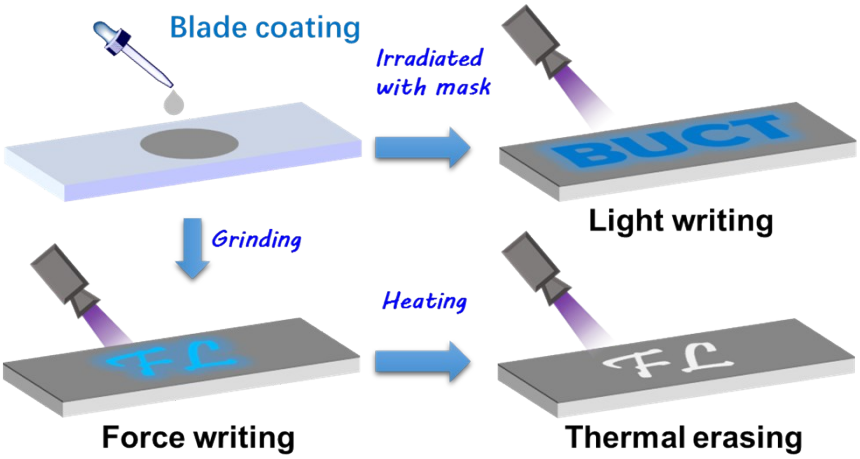

Figure S25. Preparation processes of the fluorescent information storage devices by blade coating of CSEt microcrystal.

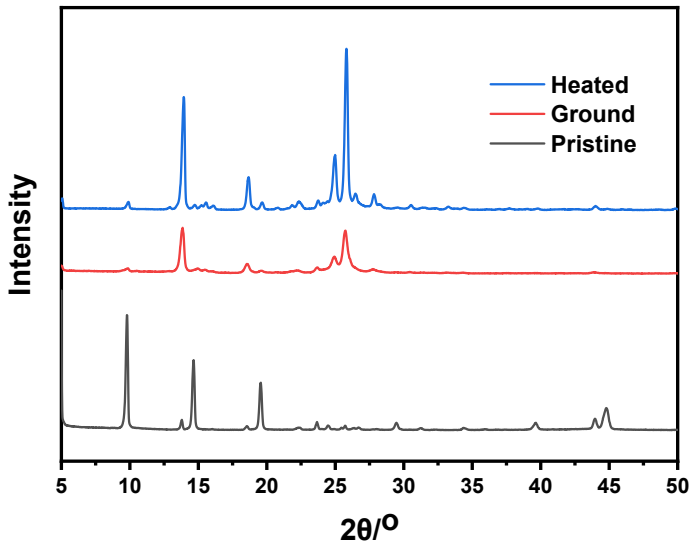

Figure S26. XRD patterns of CSEt microcrystal in different condition: pristine crystal (black line), ground powder (red line) and heat ground powder (blue line).

Comparing to the pristine CSEt crystal, the intensity of diffraction peaks of ground CSEt powder are sharply weakened, indicating the destroyed crystal structure. After treated by heating, the intensity of diffraction peaks are enhanced, indicating that the destroyed lattice could be partially recovered by heating.

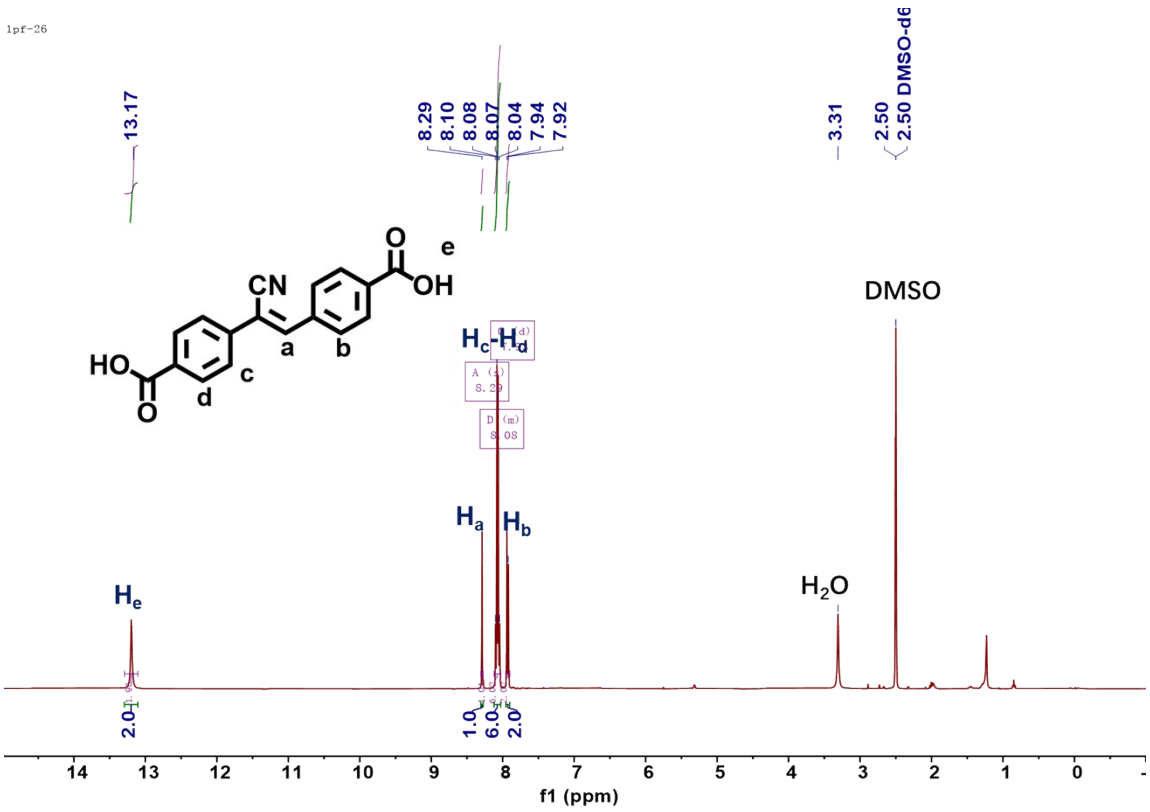

Figure S27. ^{1}H NMR spectrum of CS-COOH (DMSO-d_6).

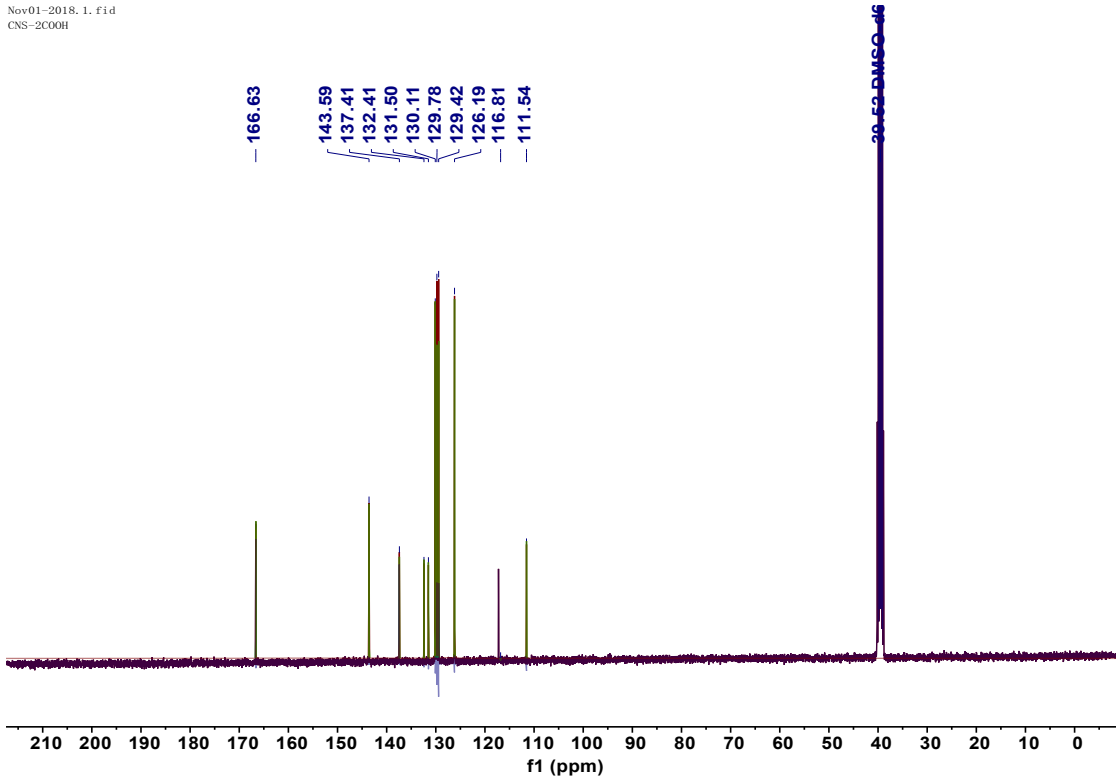

Figure S28. ^{13}C NMR spectrum of CS-COOH (DMSO-d_6).

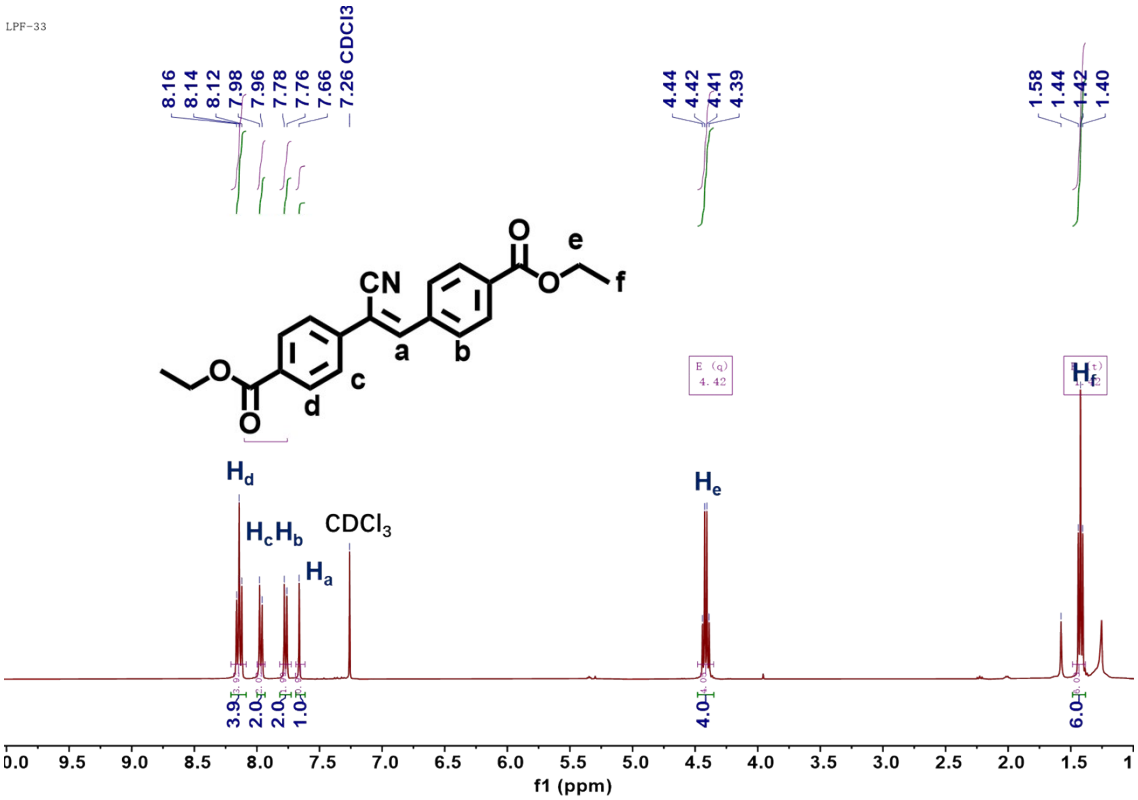

Figure S29. ^{1}H NMR spectrum of CSEt ($CDCl_3$).

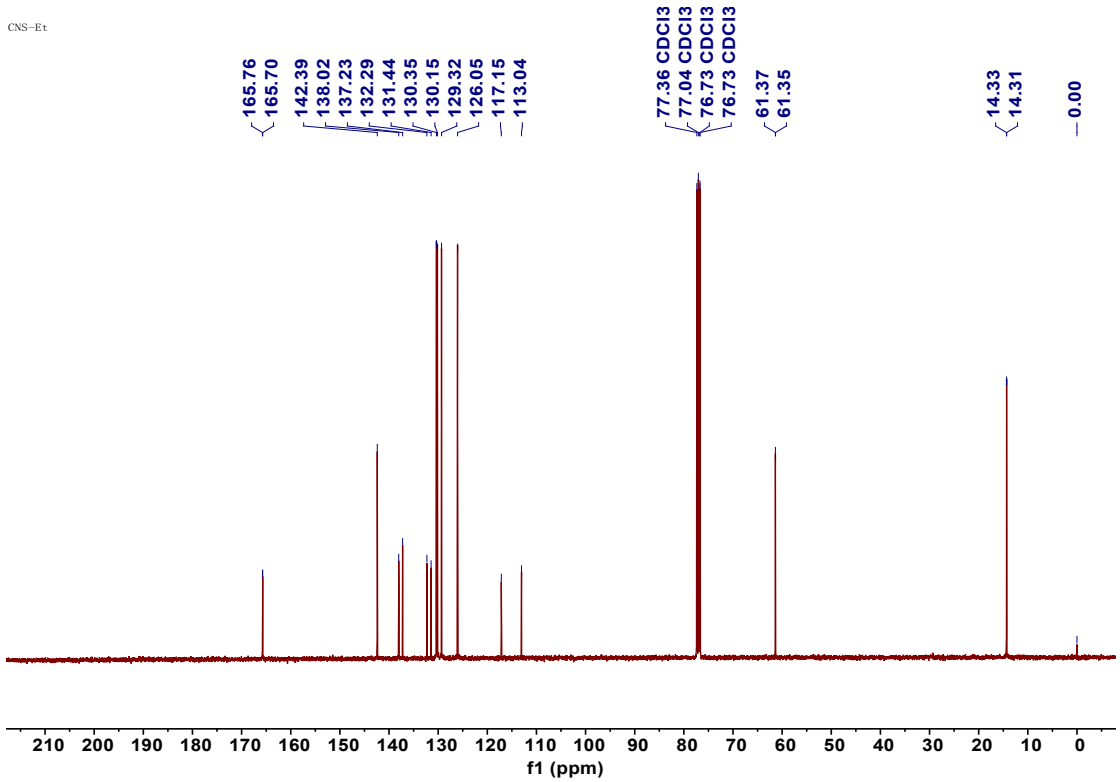

Figure S30. ^{13}C NMR spectrum of CSEt ($CDCl_3$).

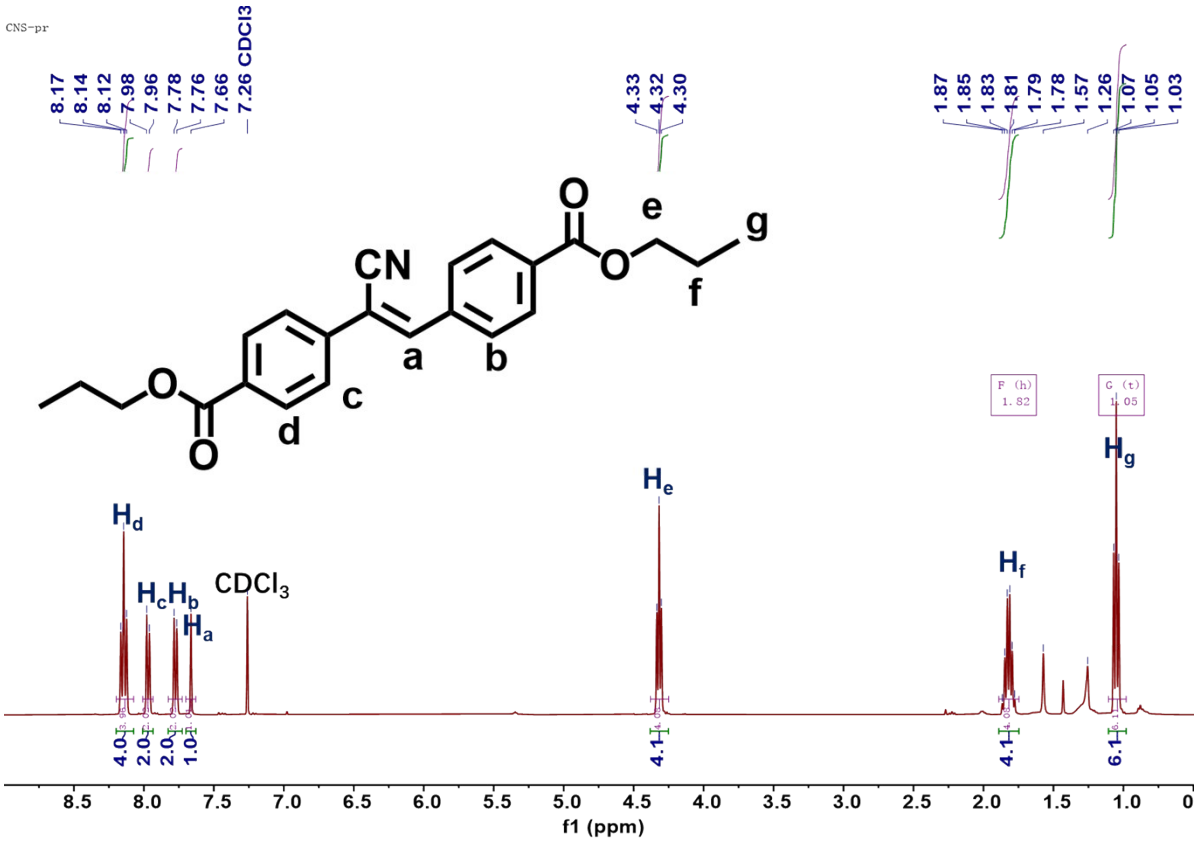

Figure S31. ^{1}H NMR spectrum of CSPr ($CDCl_3$).

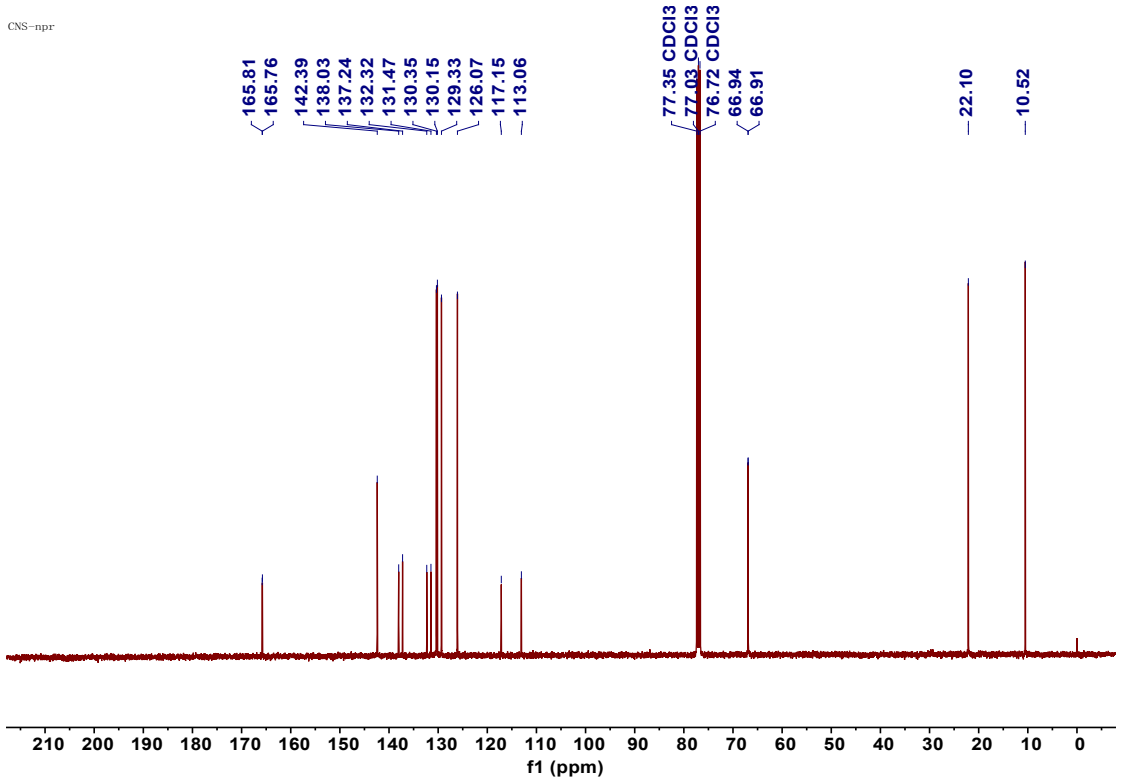

Figure S32. ^{13}C NMR spectrum of CSPr ($CDCl_3$).

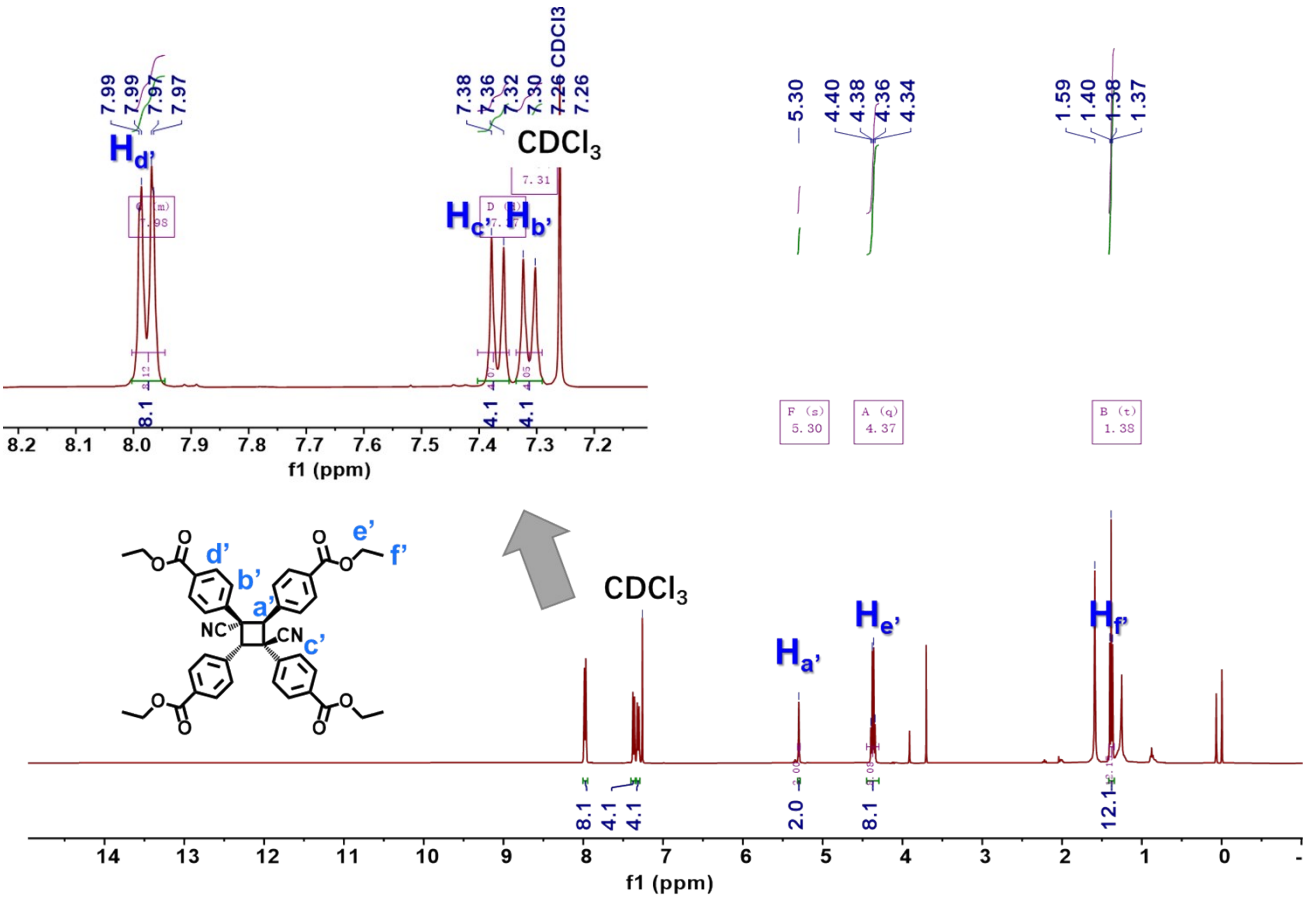

Figure S33. ^{1}H NMR spectrum of *d*-CSEt ($CDCl_3$).